Pergamon

PII: S0021-9169(96)00160-2

Journal of Atmospheric and Solar-Terrestrial Physics, Vol. 59, No. 13, pp. 1611–1623, 1997

1364-6826/97 $17.00 + 0.00

Post-sunset wintertime 630.0 nm airglow perturbations associated with gravity waves at low latitudes in the South American sector

J. H. A. Sobral,[1] G. L. Borba,[2] M. A. Abdu,[1] I. S. Batista,[1] H. Sawant,[1] C. J. Zamlutti,[1] H. Takahashi[1] and Y. Nakamura[1]

[1]Instituto Nacional de Pesquisas Espaciais-INPE, C. P. 515, 12201-970, São José dos Campos, S.P., Brazil; [2]Universidade Federal do Rio Grande do Norte-UFRN, Campus Universitário, Natal, RN, Brazil

(*Received* 19 *September* 1995; *accepted* 9 *September* 1996)

Abstract—We report photometric southern hemisphere wintertime perturbations of the nocturnal F-region atomic oxygen 630 nm red line intensity which are observed to occur concurrently with apparent ionogram signatures of F-region gravity waves. Such airglow events were detected on a total of 40 days of experiments. The airglow experiments were run at Cachoeira Paulista (CP, geographic 22° 41' S, 45° 00' W, dip 28° S). The events are characterized by south–to–north travelling airglow valleys, or depletion events (SNE). They were obtained from a set of 299 experiments performed during the period of 10 August 1977 to 4 July 1984. Their equatorwards velocities, wavelengths and periods vary within the ranges of 150–300 m s^{-1}, 100–200 km and 15 min – 3 h, respectively. They appear during the post-sunset period and remain within the field of view of the meridional scanning photometer from about ten minutes to a few hours. The SNE were seen to occur more frequently in July and were absent from September to March. The photometer scanned ±75° around zenith in the magnetic meridional and zonal planes. Ionogram spread-F and VHF polarimeter data that showed no phase or amplitude scintillations during the SNE indicated no concurrent existence of equatorial plasma depletions. It is shown that the SNE are not necessarily related to geomagnetic disturbed conditions. The present results are, to the authors' knowledge, the first showing gravity wave effects, near the sunset side of the solar terminator, on the low-latitude F-region atomic oxygen red nightglow under undisturbed geomagnetic conditions. The characteristics of these waves point to the solar terminator as their source of generation. A series of physical and morphological features of the phenomena are presented. © 1997 Elsevier Science Ltd

INTRODUCTION

Gravity wave effects on the dynamics of the ionospheric F-region have been extensively studied during the last three decades by means of radiowave probing of the ionosphere utilizing ionosondes, polarimeters, and backscatter radars (e.g. Baker and Gledhill, 1965; Bowman, 1968; Thome, 1968; Testud and Vasseur, 1969; Georges, 1968; Richmond, 1979; Abdu *et al.*, 1982; Argo and Kelley, 1986; Bowman and Monro, 1988; Crowley and McCrea, 1988; Yinn-Nien and Kang, 1991; Mishin *et al.*, 1991).

The fundamentals of gravity wave theory for the lower and upper atmosphere regions were initially established by Hines (1960) and were gradually improved through a vast number of theoretical studies (Hooke, 1968, 1970; Francis, 1974; Tuan *et al.*, 1979; Booker, 1979; Hines and Tarasick, 1987; Deminov and Deminova, 1988; Tarasick and Hines, 1990; Makhlouf *et al.*, 1990). Porter *et al.* (1974) in a theoretical simulation showed that gravity waves can modulate the zenith OI 630 nm night airglow emission rate. But so far very few studies on F-region gravity waves have utilized such airglow data. Misawa *et al.* (1981) reported simultaneous variations of the zenith OI 630 nm and OI 557.7 nm intensities at Yokosuka (35° 15' N, 139° 44' E) during auroral substorms.

The intensity of the atomic oxygen red line has been used in several phenomenological studies of the F-region, such as the dynamics of the intertropical red arc (Barbier, 1965), equatorial plasma depletions (Sobral *et al.*, 1980a,b, 1981, 1985; Sobral and Abdu, 1990, 1991) and many other phenomena. However, the phenomenon focused upon here is different from those reported before.

The OI 630 nm emission has been monitored at CP by means of a ground-based meridional scanning photometer since 1976 as part of a routine observation schedule which consists of about 13 nights of experiments per month centered on the new moon day. In 1978 a second photometer system scanning the magnetic zonal direction was added to the existing one with the purpose of complementing the meridional scanning experiments with east–west scans. The two

scanning photometers have been utilized since then in more than 1 000 nights of measurements that have resulted in contributions to the knowledge of the ionospheric dynamics over the Brazilian low-latitude region. Among those contributions are the first detection of equatorial plasma depletions in the Brazilian region (Sobral *et al.*, 1980a,b, 1981) and extended studies of that phenomenon (Sobral *et al.*, 1985; Sobral and Abdu, 1990, 1991). Sobral *et al.* (1980a,b) have shown that the bubble signatures on the meridional airglow profiles over CP consist of polewards travelling airglow depletions, or valleys, which result from the vertical and eastwards displacements of the magnetic flux-tube-aligned plasma depletions.

The signatures of those irregularities on the OI 630 nm airglow over CP have been well established through extensive studies over the past 15 years (Sobral *et al.*, 1980a,b, 1981, 1985, 1990, 1991; Sahai *et al.*, 1981; Abdu *et al.*, 1987). The polewards and eastwards propagating valleys in the airglow scan data represent depletions that may often exceed the figure of 90%. It has also been established that these valleys are always accompanied by very intense spread-F events in the ionograms and VHF scintillation in the polarimeter records over CP.

We report here the detection of a class of south–to–north travelling airglow perturbation events, or SNE, which seem to be associated with gravity waves generated near the terminator zone. This is the first report, to the authors' knowledge, of gravity wave effects on the nocturnal F-region atomic oxygen red line intensity at low latitude, near the sunset terminator. The horizontal projection at 300 km altitude of the area scanned by the 5° field of view of the photometer is shown in Fig. 1. The typical morphology of the SNE and associated dynamical features of the nocturnal ionosphere are presented and discussed in this paper.

THE SCANNING PHOTOMETERS

Each photometer utilized a 630 nm interference filter which operated at two predetermined wavelengths, one of them corresponding to a background wavelength a few nm away from 630 nm and the other at 630 nm (Sobral *et al.*, 1980a,b). Figure 2(a) and Fig. 2(b) show sets of successive meridional profiles of the OI 630 nm nightglow intensity. Each profile corresponds to a continuous photometer scan, ranging from 75° south to 75° north of zenith. The airglow intensity is the vertical displacement of the profile with reference to the background intensity level, represented by the short horizontal line segments that are shown in the flanks of the profiles. The ±75° scanning range around zenith corresponds to a latitudinal range of ±8°, or ±900 km from the zenith at 300 km altitude. The period of each scan has been set to varied values during the 7 yr period in which the experiments have been performed, ranging between 3.5 min and 5 min. The background scanning during each cycle took only approximately 30 s. The airglow signal is registered in the south–to–north sweep whereas the background signal is registered in the return sweep.

OBSERVATIONS

Table 1 shows characteristic data of the SNE: observation days (column (a)), the time range during which the perturbed airglow features remained observable in the scanning profile (b), their time duration, in minutes, (c), the sum of the 3-hourly *Kp* index for the corresponding day (d), the highest *Kp* index value of the day (e), and the *Ap* index (f). Ionosonde and polarimeter data were available for all but 7 days and 3 days, respectively, as indicated in the table.

Sobral *et al.* (1980a,b, 1981) have reported durations of several hours for the polewards moving plasma depletion structures. Those of the SNE last less, typically ranging from 10 min to 1 h. Neither phase and/or amplitude scintillation nor spread-F were seen to accompany the SNE. During the SNE the ionogram traces are interference-free from either range or frequency range spread-F, and so the quality of the ionograms has permitted a reliable determination of the reflection heights.

The 40 SNE events (one event being counted as one day of detection of the SNE event) considered here came from a set of 299 days of observations. Table 2 shows the number of experiments conducted during each of the months and years indicated in the table, including those experiments in which the SNE have not been detected. Very often, the airglow east–west profiles measured simultaneously with the north–south profiles did not present signatures during the occurrence of the SNE, except in a few cases, which is rather surprising. This aspect contrasts with the pronounced plasma depletion eastward propagating valleys (Sobral *et al.*, 1991).

RESULTS

Some examples of the SNE events that occurred on the days 7 and 13 August 1983 are presented in Figs 2 and 3, respectively. A northwards propagating valley (indicated by a dashed line) is clearly seen in the meridional scan data of Fig. 2, whereas several such propagating valleys were recorded on the night of 13

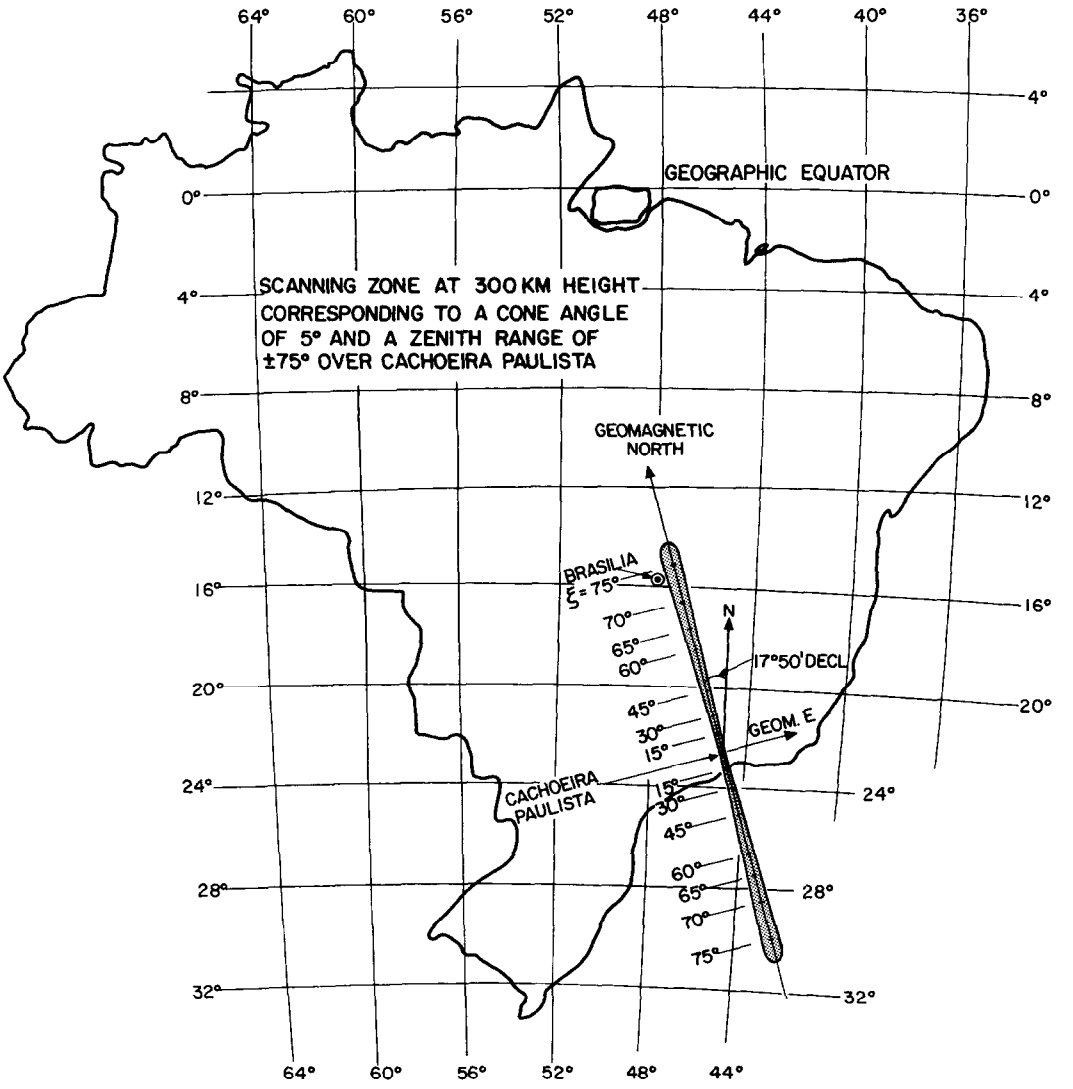

Fig. 1. The scanned region at 300 km altitude corresponding to the photometer field of view of 5° from ground at Cachoeira Paulista (CP). The angles indicated are zenith distances ξ, along the magnetic north–south direction, from the vertical direction over CP.

August as shown in Fig. 3. Although the northwards propagation of the airglow valleys is clearly evident in these figures, the amplitude of the valleys is not as remarkable as in the case of plasma depletion events (characterized by a southwards propagation) reported by Sobral *et al.* (1980a,b, 1981). In contrast with the meridional propagation of the valleys, the zonal scan observations, also shown in Figs 2 and 3, did not detect any propagating valleys. It is possible that the east–west dimension of the valleys was too large to be detected in the spatial scale sampled in the photometer's scan.

Ionogram data from CP were available for 33 out of the 40 SNE listed in Table 1. Since no spread-F activity accompanied the SNE, the clear ionogram traces permitted construction of isoionic (fixed frequency) curves in $h'F$ vs local time, some examples of which are presented in Fig. 4. The horizontal bar in each of the panels represents the time interval of occurrence of the SNE. The SNE of Fig. 2 for the night of 7 August 1983 can be identified as a gravity wave event, characterized by a downward phase propagation in the isoionic lines (Hines, 1965; Abdu *et al.*, 1982), from approximately 18 LT to 21 LT, in

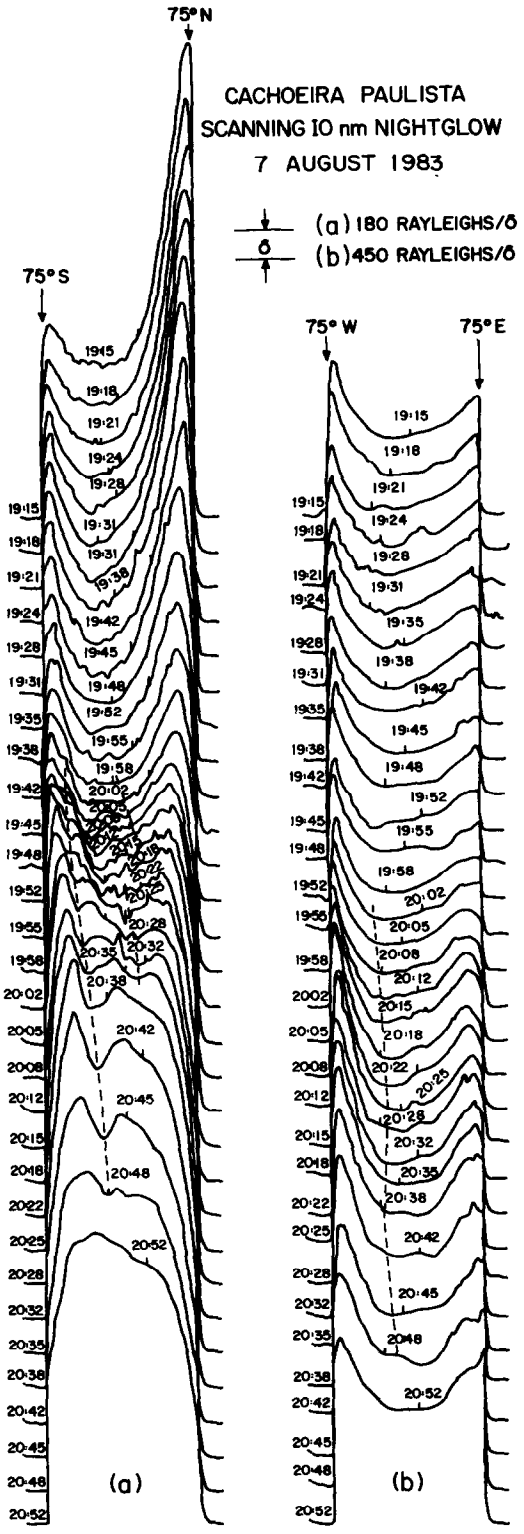

Fig. 2. Sequence of meridional profiles of the OI 630 nm nightglow intensity, along the magnetic north–south and east–west vertical planes, over Cachoeira Paulista on 7 August 1983. Each profile consists of the meridional profile of the atomic oxygen red line intensity itself (the high level between the arrows indicating 75° N and 75° S) and the background intensity (the short horizontal lines in the flanks). The patches of the south-to-north propagating events (SNE) are indicated by dashed lines. The times indicated are local time.

the panel (e) of Fig. 4. All the other SNE marked in the other panels of Fig. 4 are also accompanied by gravity wave manifestations in the $h'F$ curves. Perturbations in the isoionic contours similar to those of Fig. 4 were generally observed during the occurrences of SNE events over CP. The gravity wave signatures in the isoionic curves of Fig. 4 occur within the same time frame as do the SNE. Such signatures may be apparent before the SNE such as, for example, the SNE of 15 July 1983 (Fig. 4(d)).

The monthly occurrence statistics from April to August for the years from 1977 to 1984 are presented in Table 3, and the total number of events observed during these years are plotted in Fig. 5 as a function of month. A maximum occurrence (21 events) is found in July and only one event registered in April, with intermediate values, 3, 5, and 10, respectively, in May, June and August. The optical observational conditions vary very markedly, depending upon the season, over CP, the weather conditions being less favourable from October to March and specially during January and February. Most favourable weather conditions occur in July. This fact, however, does not explain the maximum in the SNE observed in this month, as can be verified in Table 4, which shows a July maximum also in the percentage occurrence of the SNE. Here, the percentage attributed to a given month is considered with respect to the total of 40 airglow observing days for the same month during the years 1977 to 1984. Thus the winter (July) maximum in the occurrence of the SNE events appears to be a rather pronounced real effect.

A plot of the frequency of occurrence of the SNE vs the yearly mean solar sunspot number is presented in Fig. 6. There is a tendency for the number of the SNE to increase with increasing solar activity, with the exception of the 1983 data point. Such a tendency may be partly due to the larger nightglow intensities during higher solar activity periods, permitting easier detection of the SNE. Sahai *et al.* (1988) have reported average airglow intensities about seven times higher during a solar maximum than during a solar minimum over CP. An examination of Table 1 shows that the

Table 1. (a) Date of observation of the SNE; the asterisk and double asterisk indicate unavailable ionogram and polarimeter data, respectively; (b) occurrence time range of the SNE; (c) net time of observation (minutes) of the SNE according to the previous column; (d) daily sum of the 3-hourly *Kp* index; (e) maximum 3-hourly *Kp* index of the day; (f) *Ap* index. Source for the *Kp* and *Ap* indices: *J. geophys. Res.* "Geomagnetic and Solar Data"

(a)	(b)	(c)	(d)	(e)	(f)
1 10 Aug 77	2200–2217	17	9−	2	4
2 15 Aug 77	2200–2210	10	15+	4−	11
3 5 May 78	2202–2230	28	18+	4−	10
4 26 Jul 78	1936–2013	37	14	3	7
5 27 Jul 78	2218–2245	27	10	2+	5
6 28 Jul 78	2148–2205	17	14	3−	7
7 29 Jul 78	1942–2100	1h18	13−	4−	8
8 21 May 79	1914–2036	1h22	20−	4−	13
9 27 May 79	2148–2205	17	25+	4−	17
10 18 Jun 79	1839–2225	3h46	12+	2+	6
11 19 Jun 79	1847–2205	3h18	13	3−	6
12 21 Jun 79	1918–2014	56	23+	3	15
13 20 Jul 79	1924–1945	21	24+	5−	18
14 21 Jul 79	2022–2052	30	18+	3−	9
15 27 Jul 79	1945–2041	56	27+	5+	23
16 8 Jul 80	1854–1958	4	22−	4	14
17 9 Jul 80 *,**	1922–2105	43	16−	3−	8
18 4 Aug 80 *,**	1913–2058	1h45	15	3+	8
19 5 Aug 80 *,**	1923–2154	2h31	9	1+	4
20 1 Jul 81	2127–2300	33	25+	4	17
21 27 Jul 81	1840–1901	21	28+	5−	24
22 30 Jul 81	1843–1917	34	18	3−	9
23 3 Aug 81	2121–2300	39	26−	4+	18
24 4 Aug 81	1938–1956	18	18−	4	11
25 2 Apr 82	2350–0010	20	37+	5+	20
26 15 Jul 82 *	1900–1934	34	36	5	36
27 20 Jul 82 *	1915–2000	45	25−	5+	24
28 22 Jul 82 *	1930–2020	50	22+	5−	16
29 13 Jun 83 *	2015–2310	2h55	42	8−	70
30 9 Jul 83	2020–2140	1h20	21	4−	12
31 10 Jul 83	1921–2201	40	10−	2	5
32 14 Jul 83	0000–0028	28	24−	5	19
33 15 Jul 83	2059–2104	5	10	2	5
34 3 Aug 83	1922–1946	24	24+	4−	17
35 7 Aug 83	1930–2050	1h20	20	6	18
36 8 Aug 83	1930–2040	1h10	34+	8−	62
37 13 Aug 83	2029–2335	3h16	30−	5	25
38 24 Jun 84	2120–2240	2h20	24	6−	22
39 1 Jul 84	2009–2057	48	21	5	14
40 4 Jul 84	2334–2220	46	20+	4−	12

Table 2. The days of the airglow observations concerned in this work from 10 August 1977 to 4 July 1984 (see text)

	1977	1978	1979	1980	1981	1982	1983	1984	Total
April	0	12	5	10	6	11	7	4	55
May	1	10	5	10	13	7	9	10	65
June	0	5	3	11	11	7	5	11	53
July	1	8	4	13	11	15	13	10	75
August	9	4	2	9	11	0	12	4	51
Total	11	39	19	53	52	40	46	39	299

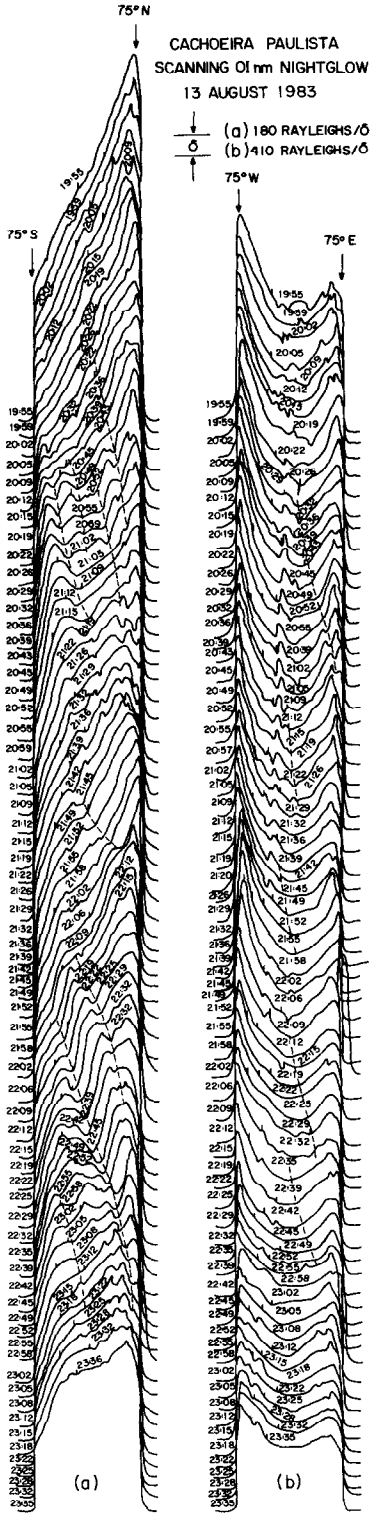

Fig. 3. The same as Fig. 2 for 13 August 1983. Several tracks are indicated by dashed lines. Notice the several patches observed on this day.

highest intensities of magnetic disturbance, of all the years, occurred in 1983 (especially in July and August), which might explain the largest number of SNE observed during this year.

An important feature of the SNE that distinguishes itself from that of the plasma bubbles is the duration of the events. Figure 7 shows the number of SNE as a function of the duration for which they appear in the meridional scan data. Each 10 min bin in this figure contains the number of SNE that occurred in the period 1977–1984. This plot clearly shows the most common duration to be of the order of 10 to 50 min. In a few cases the duration was larger than 100 min and in one case it exceeded 3 h. It is important to note that these durations are significantly shorter than those of the plasma bubble signatures in the meridional scan data over CP.

Considering the facts that the SNE result from the modulation of the airglow intensity by gravity waves, the shorter periods of the oscillations in the airglow intensity (of the order of a few tens of minutes) associated with these events would suggest that the source of these gravity waves could be the solar terminator. This hypothesis is tested by plotting in Fig. 8 the statistics of the number of initiations of the SNE events as a function of their time delay with respect to the sunset time. The number of events are counted in one-hour bins after the sunset. The entire data set considered in this work, that is, from April to August and from 1977 to 1984, is included in this figure. This figure shows considerable concentration of events initiating within the 18:30–19:30 local time period, thereby suggesting the possibility that the SNE could indeed have their origin around the terminator zone.

The possible dependence of the SNE occurrence on the magnetic disturbance is examined in Fig. 9 by plotting the number of observed events as a function of ΣKp intervals considered in increments of four units. There is a tendency for the SNE to occur more often with ΣKp increasing up to around 25. Thereafter, the number of occurrences decreases. This decrease is perhaps due to the fact that the incidence of ΣKp values higher than 25− was much less frequent than that of the ΣKp values lower than 25− during the interval of the SNE observation. Thus, while the positive dependence of the SNE on ΣKp could be real up to $\Sigma Kp \cong 25$, the negative trend seen for higher ΣKp values may not represent reality.

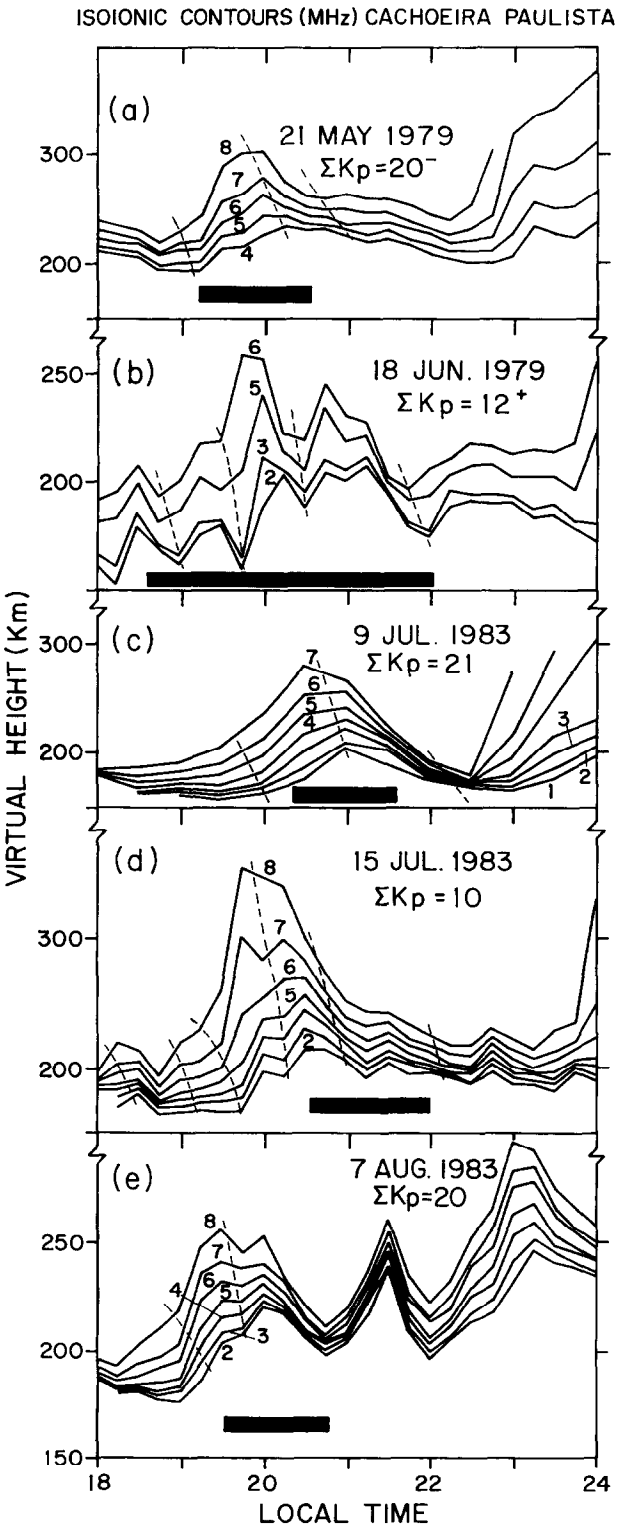

Fig. 4. Isoionic contours on the days indicated, at CP. The vertical axis shows virtual heights from ionograms recorded at CP, at integral values of frequencies in MHz. The horizontal bar indicates the presence of the SNE. The dashed lines point out the downwards phase propagating perturbations of the isoionic contours.

Table 3. Number of observations of the SNE per year and per month (see text)

	1977	1978	1979	1980	1981	1982	1983	1984	Total
April	0	0	0	0	0	1	0	0	1
May	0	1	2	0	0	0	0	0	3
June	0	0	3	0	0	0	1	1	5
July	0	4	3	2	3	3	4	2	21
August	2	0	0	2	2	0	4	0	10
Total	2	5	8	4	5	4	9	3	40

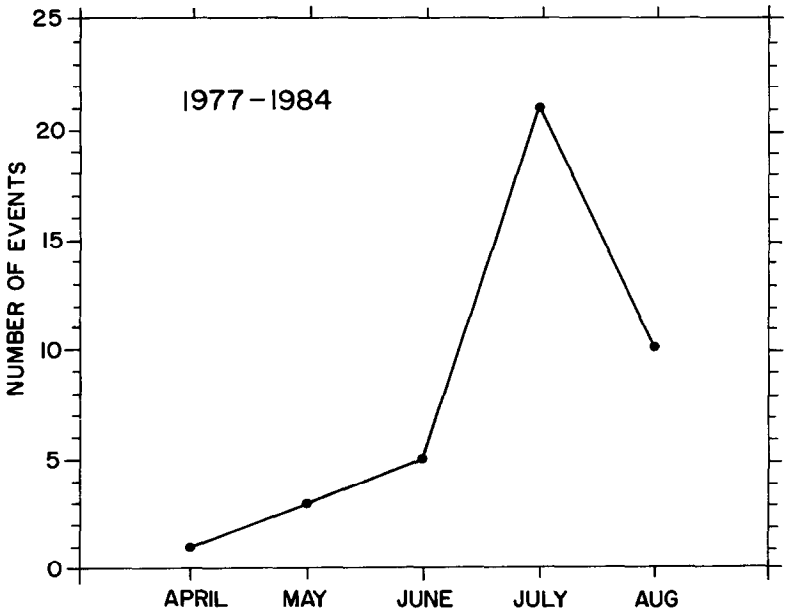

Fig. 5. Number of observations of the SNE (see caption of Fig. 2) per month for the period 1977–1984. The number of SNE is seen to be clearly seasonally dependent in this plot, maximizing in July with 21 cases of SNE observation.

Table 4. (a) Number of days of observations of the SNE; (b) total number of days of experiments; (c) column (a) divided by column (b)

	(a)	(b)	(c)
April	1	55	1.8%
May	3	65	6.2%
June	5	53	9.4%
July	21	75	28.0%
August	10	51	19.6%

DISCUSSION

Although the airglow intensity variations in the meridional scan data for the SNE could resemble those of the plasma bubble signatures, there are the following distinct features that clearly identify them as a different class of events:

(a) Their apparent meridional displacement is from south to north (equatorwards), whereas that of the plasma depletions are from north to south (polewards);

(b) The amplitudes of the airglow intensity fluctuations of the SNE are generally smaller than those produced by plasma bubbles;

(c) They are not associated with the concurrent occurrence of spread-F in ionograms and scintillation in the VHF–UHF propagation path that accompany plasma bubble events;

(d) Periods of airglow fluctuations associated with them are much shorter (Fig. 6) than those associated with plasma bubbles;

(e) They occur during the winter season, April–August, whereas plasma bubbles occur during equinoctial–summer months (Sobral *et al.*, 1980a,b, 1981; Sobral and Abdu, 1990, 1991; Abdu *et al.*, 1992); and

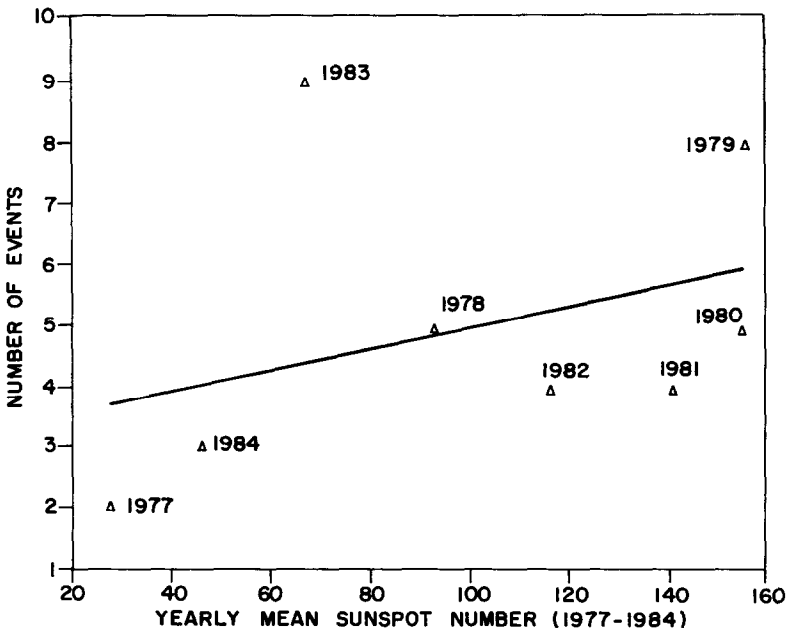

Fig. 6. Number of observations of the SNE (see caption of Fig. 2) vs yearly mean sunspot number for the period 1977–1984. The number of events tends to increase with solar activity which may be explained by the fact that during a solar maximum the SNE become more easily detectable because of increased OI 630 nm airglow intensity (see Sahai *et al.*, 1988).

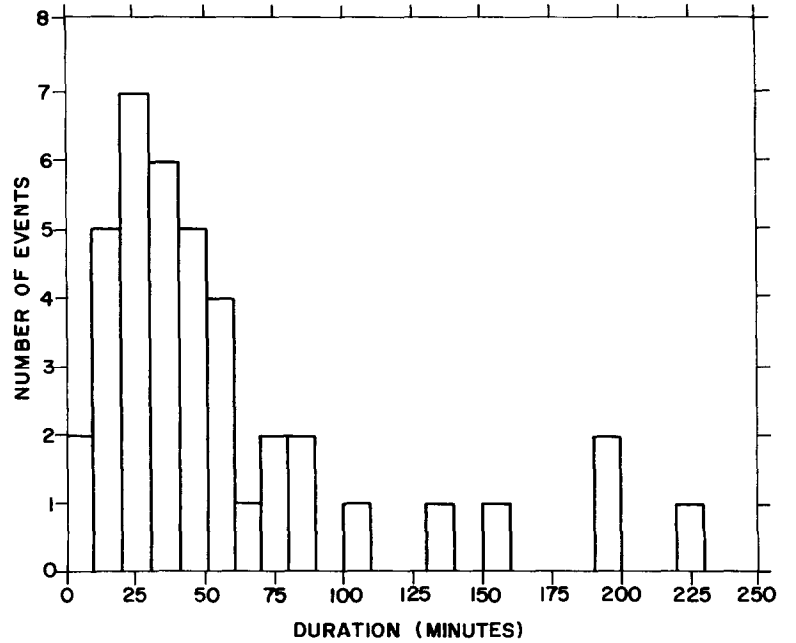

Fig. 7. Duration of the SNE: number of observations of the SNE (in the period 1977–1984) vs their respective duration in 10 min bins, where the duration is defined here as the time that the SNE remain observable within the scanning range of the airglow photometer. The total number of events (y-axis) is 40. Each of these events corresponds to one of the 40 nights in which the SNE were observed.

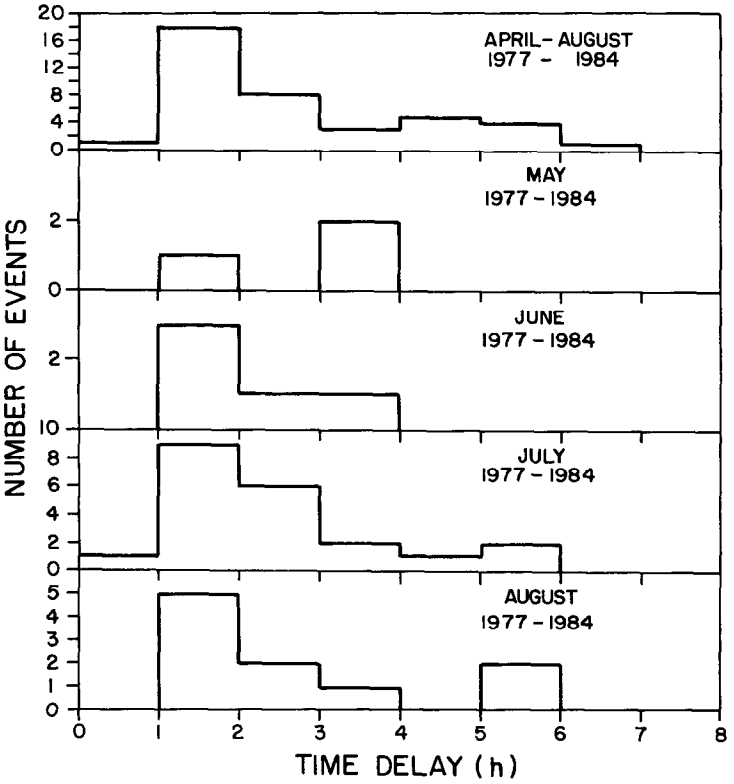

Fig. 8. Time delay of the occurrence of the SNE with respect to the sunset time. The vertical axis shows the number of observations of the SNE. The horizontal axis shows the time after sunset, in 1 h bins, when the SNE appear in the photometer scan data.

(f) Their signatures are dominant in the meridional scan data and hardly perceptible in the zonal scan data, whereas the plasma bubble signatures are clearly detectable in either of the scan modes.

Having thus established the identity of SNE as clearly different from that of plasma bubbles, we now examine the evidence for their being a manifestation of gravity wave modulation of the 630 nm airglow intensity. The results in Fig. 3 provide statistical evidence that they are indeed associated with perturbations in intensity contours of plasma frequency (as obtained by the ionosonde at CP). The downwards phase propagation of these disturbances is a rather clear indication of the presence of gravity waves.

If they do indeed represent gravity wave signatures of the airglow meridional scan data then the question arises as to what could be the source of these waves. The results in Fig. 8 show that the occurrence of these events steadily decreases with increasing distance from the terminator, becoming almost negligibly small around midnight hours, in all months except in May. The largest number of occurrences observed within 1–2 h from sunset could suggest that these waves could be generated at the terminator. The impossibility of making airglow measurements closer to the sunset hours makes it difficult to determine the occurrence of the disturbances closer to the terminator. Nevertheless, the evidence in Fig. 7 does seem to point to a gravity wave source close to the terminator. The lack of any clear dependence of the number of SNE on the ΣKp values shown in Fig. 9 would seem to rule out magnetic (auroral) activity as a possible source of these waves. It might be asked then why these terminator associated gravity wave signatures, in the form of SNE, are observed in winter and not during the equinoxes and summer. In this connection it could be argued that, in the spread-F occurrence season, that is, in equinoctial and summer months, when the ambient sunset ionospheric conditions are propitious for instability growth, an initial perturbation in the form of a gravity wave could trigger a spread-F event (see Kelley, 1989), so that the ensuing plasma bubble signature of a sufficiently large amplitude could domi-

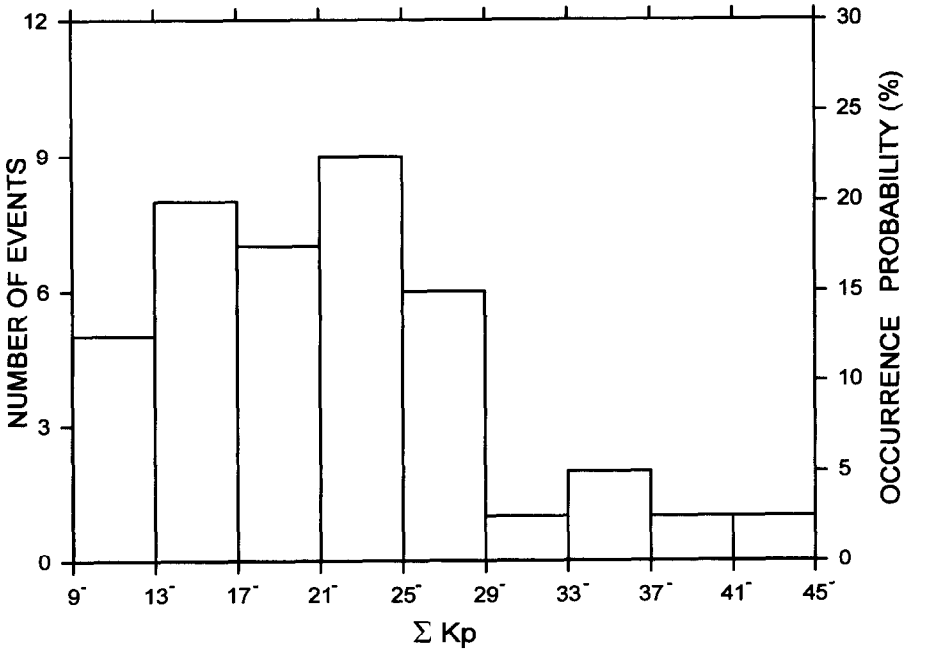

Fig. 9. Number of observations of the SNE vs the daily sum of the 3-hourly *Kp* index. Most of the observations of the SNE have occurred in the ΣKp range below 29−.

nate the fluctuations observed in the airglow data. Under this condition, only the northwards propagating airglow valleys that are characteristic of plasma bubbles are observable. It may be possible that occurrences of SNE in the F-region are controlled by the direction of neutral winds in the mesosphere and lower thermosphere. Gravity waves can propagate upwards only when the propagation direction of the gravity waves is opposite to the neutral wind direction. Such a condition can be satisfied in the winter months.

The fact that the zonal scan (magnetic east–west direction) data, in Figs 2(b) and 3(b), show no significant propagating disturbance might suggest that the phase of the propagating wave is approximately aligned with magnetic east–west within the scanning range. We do not understand the reason for this situation. However, it is worth noting that the large magnetic declinations of Cachoeira Paulista (20°W) would make the angle between the terminator and the magnetic east–west direction over this location in winter deviate much more than for any other low-latitude location over the globe (by around 41°). One factor that could obviously contribute to the stronger perturbation signatures in the meridional plane as compared to the zonal plane may be the magnetic field alignment of the rarefactions. For example, when the photometer looks along the geomagnetic field lines, during a meridional scan, the effect of field-aligned plasma depletion (or enhancement) could result in a decreased (enhanced) nightglow intensity. In the zonal scanning mode the photometer never looks along the field line.

CONCLUSION

This is the first report of the detection of gravity wave signatures over Cachoeira Paulista (CP) utilizing OI 630 nm airglow as a diagnostic technique. More than 1 000 nights of measurements were performed during the period of 1976–1995 and the results show clearly that the F-region perturbations can be rather sensitively tracked by the CP scanning photometer system. We have analyzed 40 events of south–to–north propagating wavelike perturbation events (SNE) that occur during the early post-sunset hours. They occur as isolated events in contrast with the well-known perturbations associated with plasma bubbles which are accompanied by spread-F and scintillation events and which propagate southwards in the airglow meridional profiles. They occur only in the winter, with maximum in July, in contrast with the plasma bubbles which occur in the equinoctial and summer months over CP. These and other important characteristics establish their identity as distinct from that of plasma bubble events. This identification as signatures of gravity waves is supported by their occurrence always

being associated with an oscillation in the isoionic lines observed from ionograms. The period of oscillation (< 1 h) of these gravity waves suggests sources of their generation rather close to their detection zone. This fact, coupled with the fact of their steadily decreasing occurrence with increasing time delay from sunset, strongly suggests their source region at the terminator. The seasonal dependence of the SNE frequency of occurrence may possibly be an indication of the control of the neutral wind directions in the mesosphere and lower thermosphere. The present results, therefore, provide, to our knowledge, the first evidence of gravity wave generation by the sunset terminator at low latitudes. Gravity waves act as a perturbation source for initiating plasma bubble events during the months when the ambient ionospheric conditions provide favourable chances for instability growth. When bubble growth takes place, the associated modulation in airglow intensity dominates the meridional scan data. However, when the ambient conditions are not favourable for bubble growth the gravity wave modulations in the airglow are registered as the south–to–north travelling events (SNE). We have not understood clearly the reason for the absence of simultaneous signatures in the zonal scan data. Studies are in progress to further our understanding of this phenomenon.

Acknowledgements—This work has been partially funded by the Conselho Nacional de Desenvolvimento Científico e Tecnológico- CNPq through grants 521980/94-1 (J. H. A. Sobral) and 500003/91.3 (M. A. Abdu).

REFERENCES

Abdu M. A., Batista I. S., Kantor I. J. and Sobral J. H. A. 1982 *J. atmos. terr. Phys.* **44,** 759–767.

Abdu M. A., Sobral J. H. A., Nakamura Y. and Zamlutti C. J. 1987 *Geophys. res. Lett.* **14,** 965–968.

Abdu M. A., Batista I. S. and Sobral J. H. A. 1992 *J. geophys. Res.* **90,** 14897–14904.

Argo P. E. and Kelley M. C. 1986 *J. geophys. Res.* **91,** 5539–5556.

Baker D. C. and Gledhill J. A. 1965 *J. Phys.* **27,** 1223–1227.

Barbier D. 1965 *Ann. Geophys.* **21,** 228–234.

Booker H. G. 1979 *J. atmos. terr. Phys.* **41,** 501–515.

Bowman G. G. 1968 *J. geophys. Res.* **93,** 721–734.

Bowman G. G. and Monro P. E. 1988 *J. atmos. terr. Phys.* **50,** 215–224.

Crowley G. and McCrea I. W. 1988 *Radio Sci.* **23,** 905–918.

Deminov M. G. and Deminova G. F. 1988 *Geomagnetism and Aer.* **28,** 185–187.

Francis S. H. 1974 *J. geophys. Res.* **79,** 5245–5260.

Georges T. M. 1968 *J. atmos. terr. Phys.* **30,** 735–746.

Hines C. O. 1960 *Can. J. Phys.* **38,** 1441–1481.

Hines C. O. 1965 *Physics of the Earth's Upper Atmosphere.* Prentice-Hall, Englewood Cliffs.

Hines C. O. and Tarasick D. W. 1987 *Planet. space Sci.* **35,** 851–866.

Hooke W. H. 1968 *J. atmos. terr. Phys.* **30,** 795–823.

Hooke W. H. 1970 *J. geophys. Res.* **75,** 5535–5544.

Kelley M. C. 1989 *The Earth's Ionosphere-Plasma Physics and Electrodynamics.* Academic Press, Inc.

Makhlouf U., Dewan E., Isler J. and Tuan T. F. 1990 *J. geophys. Res.* **95,** 4103–4112.

Misawa K., Takeuchi I. and Kato Y., Aoyama I. 1981 *Ann. Geophys.* **37,** 549–556.

Mishin E. V., Epishova A. E., Ishkova L. M., Kozlov E. F., Kolokolov L. E., Rubtsov L. N., Samorokin N. I., Sidorova L. N., Somsikov V. M., Telegin V. A. and Yodovick L. A. 1991 *J. atmos. terr. Phys.* **53,** 643–648.

Porter H. S., Silverman S. M. and Tuan T. F. 1974 *J. geophys. Res.* **79,** 3827–3833.

Richmond A. D. 1979 *J. geophys. Res.* **84,** 1880–1890.

Sahai Y., Takahashi H., Bittencourt J. A., Sobral J. H. A. and Teixeira N. R. 1988 *J. atmos. terr. Phys.* **50,** 135–140.

Sobral J. H. A., Abdu M. A. and Batista I. S. 1980 *Ann. Geophys.* **36,** 199–204.

Sobral J. H. A., Abdu M. A., Batista I. S. and Zamlutti C. J. 1980 *Geophys. res. Lett.* **7,** 980–982.

Sobral J. H. A., Abdu M. A., Batista I. S. and Zamlutti C. J. 1981 *J. geophys. Res.* **86,** 1374–1378.

Sobral J. H. A., Abdu M. A. and Sahai Y. 1985 *J. atmos. terr. Phys.* **47,** 895–900.

Sobral J. H. A. and Abdu M. A. 1990 *J. geophys. Res.* **95,** 8253–8257.

Sobral J. H. A. and Abdu M. A. 1991 *J. atmos. terr. Phys.* **53,** 729–742.

Tarasick D. W. and Hines C. O. 1990 *Planet. space Sci.* **38,** 1105–1120.

Testud J. and Vasseur G. 1969 *Ann. Geophys.* **25,** 525–546.

Thome G. D. 1968 *J. geophys. Res.* **73,** 6319–6336.
Tuan T. F., Hedinger R., Silverman S. M. and Okuda M. 1979 *J.geophys. Res.* **84,** 393–398.
Yinn-Nien H. and Kang C. 1991 *J. geophys. Res.* **96,** 13953–13966.